SCIENTIFIC REPORTS

OPEN

CONFERENCE PROCEEDINGS

APEnergy2014

SUBJECT AREAS:
ELECTRONIC DEVICES
BATTERIES

Received
6 February 2014

Accepted
14 March 2014

Published
29 August 2014

Correspondence and requests for materials should be addressed to S.M.O. (seungoh@snu.ac.kr)

* These authors contributed equally to this work.

Allylic ionic liquid electrolyte-assisted electrochemical surface passivation of $LiCoO_2$ for advanced, safe lithium-ion batteries

Junyoung Mun[1,2]*, Taeeun Yim[1,3]*, Jang Hoon Park[4], Ji Heon Ryu[5], Sang Young Lee[4], Young Gyu Kim[1] & Seung M. Oh[1]

[1]Department of Chemical and Biological Engineering, Seoul National University, Seoul 151-744 Korea, [2]Department of Energy and Chemical Engineering, Incheon National University, Incheon 406-840, [3]Advanced Batteries Research Center, Korea Electronics Technology Institute (KETI), Gyunggi-do 463-816, Korea, [4]School of Green Energy, Ulsan National Institute of Science and Technology, Ulsan 689-798, Korea, [5]Graduate School of Knowledge-based Technology, Korea Polytechnic University, Korea.

Room-temperature ionic liquid (RTIL) electrolytes have attracted much attention for use in advanced, safe lithium-ion batteries (LIB) owing to their nonvolatility, high conductivity, and great thermal stability. However, LIBs containing RTIL-electrolytes exhibit poor cyclability because electrochemical side reactions cause problematic surface failures of the cathode. Here, we demonstrate that a thin, homogeneous surface film, which is electrochemically generated on $LiCoO_2$ from an RTIL-electrolyte containing an unsaturated substituent on the cation (1-allyl-1-methylpiperidinium bis(trifluoromethanesulfonyl)imide, AMPip-TFSI), can avert undesired side reactions. The derived surface film comprised of a high amount of organic species from the RTIL cations homogenously covered $LiCoO_2$ with a <25 nm layer and helped suppress unfavorable thermal reactions as well as electrochemical side reactions. The superior performance of the cell containing the AMPip-TFSI electrolyte was further elucidated by surface, electrochemical, and thermal analyses.

As environmental threats are no longer simply fearful expectations, we are on the verge of a developing a generation of renewable energy systems that have a much lower impact on the environment than conventional energy sources, such as thermoelectric power from fossil fuels. In keeping with that aim, electric vehicles (EVs) have emerged as an alternative transportation option because of their environmental benefits. However, in order to implement them, several hurdles have to be overcome; in particular, reliable energy storage devices, which play a key role in mitigating inherent fluctuations associated with renewable energy sources, and they will need to provide high energy densities to allow EVs to travel long distances. Accordingly, lithium-ion batteries (LIB), which have undergone major advances since their implementation in small devices like mobile phones, computing devices, and power tools, are now considered one of the most promising power sources for both renewable energy systems and electric vehicles owing to their high energy density and long cyclability[1–5]. Despite those merits, a safety issue restricts their applications because LIBs are comprised of flammable components and can ignite or even explode when they are exposed to high temperatures or abnormal charging[6,7]. The undesirable thermal runaway is triggered by the exothermic decomposition of flammable components such as the carbonate electrolyte in LIBs[6,8,9]. This issue is regarded as the most critical problem in large energy reservoirs (on scales ranging from W·h to MW·h). Similarly, the cyclability of LIBs is also an important concern because replacing large-scale LIBs are cost prohibitive. Electrode failure due to surface fouling is another major concern regarding the cycle life of LIBs.

The electrochemical stability window is another concern since nearly all electrolytes are unable to support the operating potential range of LIBs; therefore, electrochemical side reactions that occur on the electrode surface during cycling are unavoidable. Following the decomposition of electrolyte, solid-type byproducts usually remain and passivate the electrode surface. An ideal surface film on the electrode would be thin and homogeneous, possess low resistivity, and prevent electrolytes from reaching electrochemically reactive sites. The film should also be a lithium conductor and concomitantly serve as an electronic insulator to avoid the electrochemical side

reactions that bring about the loss of lithium ions and increase in kinetic resistance. The surface film could also improve the thermal stability of the cell by impeding surface thermal reactions at elevated temperatures.

To promote thermal stability and inhibit continuous electrolyte decomposition on the electrode, many researchers have developed electrochemically formed surface films, namely solid electrolyte interphase (SEI), by controlling the characteristics of surface films, such as their chemical composition, thickness, and coverage[10]. However, it is still considered a big challenge to achieve a bifunctional surface modification that improves both the electrochemical and thermal aspects of the electrode[11].

The safety aspect to consider is that when cell temperatures increase beyond 150°C, thermal runaway is triggered by the exothermic decomposition of the electrolyte, and it drives the breakdown of other components in the LIBs. To prevent the explosions of LIBs, non-flammable electrolytes have been investigated for the development of safe LIBs. Specifically, room temperature ionic liquids (RTIL) have attracted much attention due to their unique nonvolatile characteristics even under ultra-high vacuum because RTILs are only comprised of ions and do not generate reactive gas-phase molecules[12,13]. RTILs consisting of pyrrolidinium or piperidinium are electrochemically stable on inert Pt and glassy carbon electrodes, but their use as electrolyte in LIB systems has been limited because of their unavoidable electrochemical decomposition on the cathode used for LIB[14–16]. Despite their wide electrochemical voltage window, surface side reactions can still occur on the cathode as well as on the anode since there exists electrochemically fragile surface groups of active materials and local uneven polarization from high viscosity[17,18].

In the present study, a thermally stable RTIL-containing piperidinium was introduced to the electrolytic solvent for the development of safe lithium-ion batteries. 1-allyl-1-methylpiperidinium bis(trifluoromethanesulfonyl)imide (AMPip-TFSI) was used as the solvent for the LIB electrolyte to build a protective film on the cathode without prematurely coating it. We then investigated the electrochemical and thermal characteristics of the derived surface films using electrochemical methods, surface analyses, and differential scanning calorimetry (DSC).

Results

Electrochemical voltage profiles. Figure 1 presents the voltage profiles for the 1st and 15th cycles as obtained from Li/$LiCoO_2$ cells with the prepared electrolytes, 1.0 M LiTFSI/PMPip-TFSI (PMPip: 1-methyl-1-propylpiperidinium) and 1.0 M LiTFSI/AMPip-TFSI, for the galvanostatic charge/discharge at a current density of 0.1 C (1 C = 140 mA·g^{-1}). A couple of long, reversible plateaus can be observed around 3.9 V, which correspond to the reversible oxidation state changes between Co^{3+} and Co^{4+} of $LiCoO_2$[16,19,20]. This demonstrates that the prepared electrolytes served as a lithium ion conductor between the electrodes to complete a closed circuit in the cell. When the same lithium salt is used, if the solvent electrolyte is less viscous, the lithium ion conductivity increases because of easier ion-migration. The presence of an allylic substituent in the prepared electrolytes reduces viscosity and improves electrolyte conductivity by reducing the molecular volume (decreasing van der Waal's forces) and weakening Coulombic interaction by delocalizing the electrons on the attached allylic group to a larger extent when compared to a saturated alkyl substituent (PMPip-TFSI: 141 cP and 2.9 mS·cm^{-1} and AMPip-TFSI: 108 cP and 3.5 mS·cm^{-1})[21,22]. With dissolving of 1 M LiTFSI into RTILs, the trend of conductivity is consistently observed (1 M LiTFSI in PMPip-TFSI: 0.42 mS cm^{-1} and 1 M LiTFSI in AMPip-TFSI: 0.46 mS cm^{-1}). The superior conductivity of the AMPip-TFSI electrolyte increased the obtained specific capacity of the cell during charge/discharge[21].

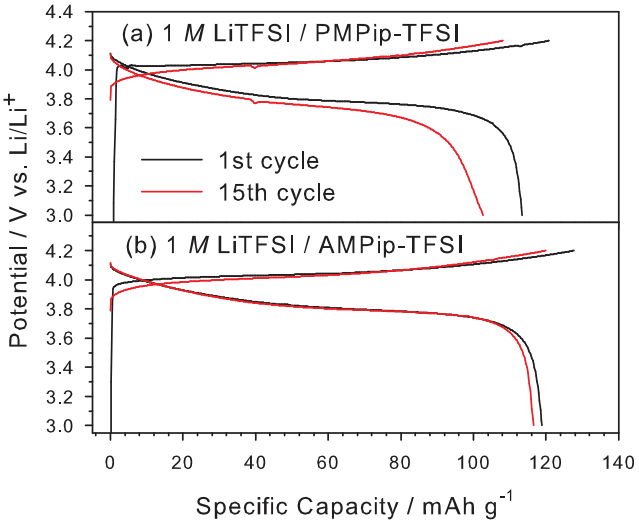

Figure 1 | The 1st and 15th galvanostatic charge-discharge voltage profiles obtained with the $LiCoO_2$/Li cell (2032-type coin cell) in two kinds of electrolyte at 25°C: (a) 1.0 M LiTFSI/PMPip-TFSI and (b) 1.0 M LiTFSI/AMPip-TFSI. Current density = 14 mA·g^{-1}. Voltage cut-off = 3–4.2 V (vs. Li/Li^+).

PMPip-TFSI provided for sustained high electrochemical reversibility of the cell during the 1st cycle since, being able to deliver 93.9% of the Coulombic efficiency of the 1st cycle (AMPip-TFSI: 93.1%). The viscous RTIL causes irreversible side reactions even at potentials under 4.2 V, where $LiCoO_2$ is highly electrochemically reversible[16,23]. The irreversible capacity could be induced by the reversible ion loss from side reactions of the electrolyte during the charging sequence or the imperfect discharge due to kinetic hindrances during discharge. Since conductivity of AMPip-TFSI is higher than that of PMPip-TFSI, the electrolyte kinetics of lithium transport is not the main reason for the low 1st cycle Coulombic efficiency. Therefore, we estimated that the irreversible capacities derived from electrolyte decomposition[16]. Therefore, a large amount of AMPip-TFSI electrolyte participates in the oxidative reactions despite its good conductivity. With glassy carbon inert electrode with the experimented RTILs, the result of cyclic voltammetry shows that the AMPip-TFSI brings higher current than the PMPip-TFSI (Supplementary #2). It represents that the AMPip-TFSI is more electrochemically fragile than PMPip-TFSI and is consistent with the low 1st Coulombic efficiency of LIB with AMPip-TFSI. On the other hand, for voltage profile of the 15th cycle, the obtained specific charge and discharge capacities were decreased owing to the high polarizations. The reasons behind high polarization are discussed in great detail in the Electrochemical analyses subsection.

Surface analyses. We expected the derived surface films to be altered as a result of the electrochemical decomposition of the electrolytes. To investigate more closely, the morphologies of the surface films on the cathode, which was cycled once in the cell, were analyzed by TEM (Figure 2a and 2b). In the bright-field TEM images, the highly dense $LiCoO_2$ powder appears as a shadowy material. The bright parts on the interface of the powder, which were generated during cycling, are clearly seen in both the samples. In the case of the PMPip-TFSI electrolyte, the surface film had the appearance of aggregated thick islands (Figure 2a); in contrast, the surface film from AMPip-TFSI homogeneously coated the electrode surface and was much thinner (<25 nm) than that from PMPip-TFSI (Figure 2b).

The surface states of the cycled electrodes were studied by XPS to examine the chemical composition and level of coverage. The surface film on $LiCoO_2$ consists of carbon and fluorine, elements abundantly present in the RTIL electrolyte. The derived surface film on the active

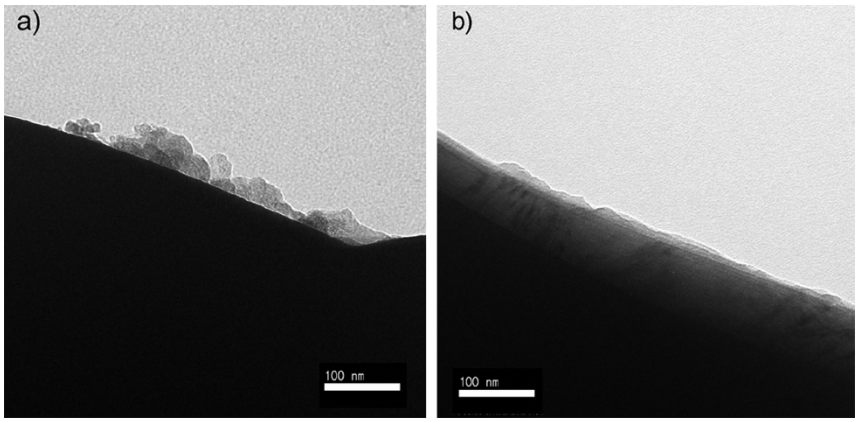

Figure 2 | TEM images of $LiCoO_2$ after 10 cycles in (a) 1.0 M LiTFSI/PMPip-TFSI and (b) 1.0 M LiTFSI/AMPip-TFSI.

material influences cell performance with respect to the lithium transportation that occurs through the film on the active material. If a conventional composite electrode with a conducting agent and binder is exposed to an X-ray beam during XPS measurements, all components emit photoelectrons and not just the active material. Clear spectra of the surface film should be obtained to investigate the surface phenomena on $LiCoO_2$. However, the photoemissions of carbon and fluorine atoms in the conducting agent (carbon nano powder) and binder (polyvinyldifluoride, PVdF) during XPS analysis make it impossible to distinguish the spectra of purely the surface films on $LiCoO_2$ by interfering with the interpretation of the passivation film. To eliminate these hindrances, pristine $LiCoO_2$ embedded onto Au foil, in which the binder and conducting agent were absent, was used for the XPS analyses[6]. From these electrodes, C1s, F1s, and $Co2p_{3/2}$ spectra were obtained and are shown in Figure 3. After a cycling both PMPip-TFSI and AMPip-TFSI electrolytes, carbon and fluorine compounds were apparently deposited onto the surface of the cathode. Regarding the photoelectrons transferred from only the top surface of the electrode, the additional spectra, with the exception of that from the $LiCoO_2$ electrode, correlate well with the TEM results.

The C1s spectra exhibited the following four assignable peaks: C–C at 285 eV, C–N at 286.5 eV, C=O and CO_3 at 289.0 eV, and CF_3 at 293.0 eV (Figure 3a and 3b). C–C and C–N peaks generated from cation decomposition were dominant in all C1s spectra, but a peak corresponding to CF_3 from the TFSI anion of RTILs was not abundant. This reveals that the surface film was developed from the cation, piperidinium, rather than from the anion during cycling. A comparison of C1s spectra showed that the photoelectrons from the electrode cycled in AMPip-TFSI exhibited a much higher intensity than those cycled in PMPip-TFSI. The calculated relative atomic ratio also supports this trend (Table 1). Formation of carbon compounds, found in the surface film formed in AMPip-TFSI electrolyte might take place in according to the electrochemically induced oxidative polymerization (see Figure S1 in Supplementary Information). Once a radical is formed in the carbon of AMPip-TFSI as a result of electrochemical oxidation, conjugation of π electrons at the ends of allylic substituent can effectively stabilize the radical intermediates. It means that the allyl group enables to stabilize the radical; therefore, it facilitates oxidative decomposition reaction of AMPip-TFSI during the electrochemical charge sequence, resulting in the formation of passivation film via intermolecular radical coupling reaction. Difference in chemical structure between AMPip-TFSI and PMPip-TFSI might be influenced to surface chemistry of positive electrode – PMPip-TFSI consisting of only sp^3-carbons substituent is relatively unfavorable owing to lack of the functionalities which enable to stabilize radical intermediate. Therefore, it was believed that the organic film passivation from PMPip-TFSI was inferior to that from AMPip-TFSI (Table 1).

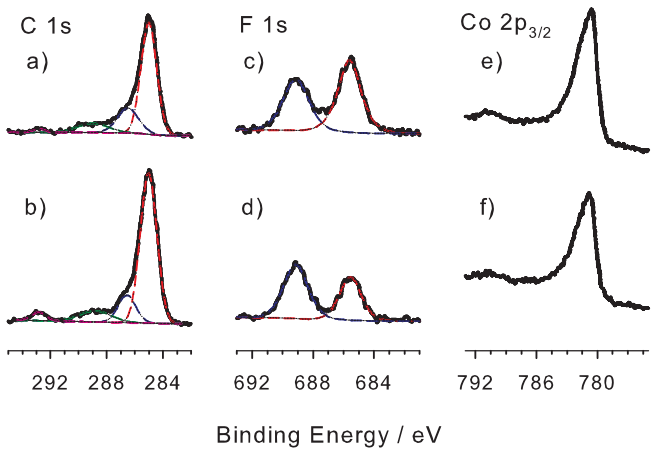

Figure 3 | XPS spectra for (a and b) C1s, (c and d) F1s, and (e and f) $Co2p_{3/2}$ from the $LiCoO_2$-embedded Au electrode after 1 cycle in different electrolytes. The upper spectra were obtained from the electrode cycled in 1.0 M LiTFSI/PMPip-TFSI, and the lower spectra were obtained from the electrode cycled in 1.0 M LiTFSI/AMPip-TFSI.

The passivation film also had fluoride-containing chemical components, such as LiF (685 eV) and CF_3 (689.6 eV), from the anions (Figure 3c and 3d). However, the relative atomic concentrations of fluoride components were much lower than those of the carbon species (Table 1). Furthermore, the amounts of fluoride from AMPip-TFSI electrolytes are relatively low due to the organic passivation effect of the AMPip cation. Specifically, LiF is considered highly resistive because it is too dense to pass lithium ions since the rate constant for the formation of LiF is high[24,25]. Consequently, the carbonaceous surface film from the AMPip cation successfully impeded the formation of a resistive fluorine film.

The photoelectrons from Co are depicted in Figure 3e and 3f. These Co spectra originate from $LiCoO_2$ based on the peak positions (780.5 eV). Furthermore, the degree of film coverage level could be confirmed by comparing the relative atomic concentration of Co from the electrode material. $LiCoO_2$, which is buried beneath the

Table 1 | Relative atomic concentrations from the XPS analyses in Fig. 3

Atomic conc.	C	LiF	Co
PMPip-TFSI	38.6	5.1	7.2
AMPip-TFSI	43.1	3.0	5.7

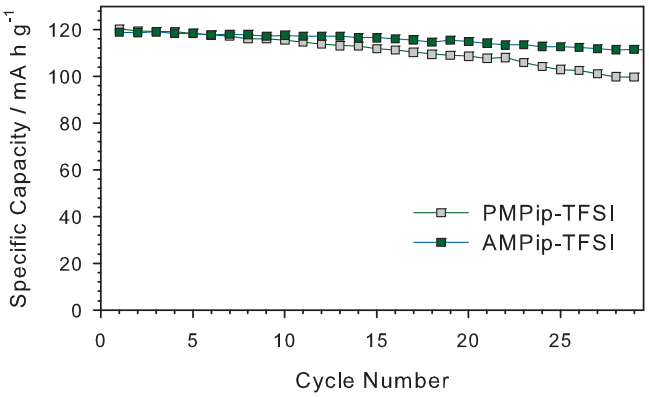

Figure 4 | Cycling performance of a $LiCoO_2$/Li cell with PMPip-TFSI and AMPip-TFSI in which 1 M of LiTFSI was dissolved. The gray squares represent PMPip-TFSI and the green squares represent AMPip-TFSI. Current density = 14 mA·g^{-1}. Voltage cut-off = 3–4.2 V (vs. Li/Li$^+$). Temperature = 25°C.

surface film, cannot contribute to the Co spectra because the photoelectrons emitted at that depth were unable to pass through the surface film. The Co atomic concentration from the electrode cycled in AMPip-TFSI (5.7%) was lower than that cycled in the PMPip-TFSI electrolyte (7.2%) (Table 1). This also supports the observation that the passivation film from AMPip-TFSI has high level of coverage. The surface film from AMPip-TFSI homogeneously covered the cathode even after the 1st cycle. It also differs from the PMPip-TFSI-derived film in that it is comprised of the organic species from cation decomposition and low fluoride content according to anion decomposition, which is characterized by the high level of coverage. All the analyses (TEM and XPS) performed indicate that the homogeneous passivation film was successfully formed on the surface by the allylic RTILs.

Electrochemical analyses. The cyclabilities of the cells with PMPip-TFSI and AMPip-TFSI are shown in Figure 4. During cycling, the specific discharge capacities of the cell with the AMPip-TFSI electrolyte were more stable than those with PMPip-TFSI. This represents that the electrochemically formed, thin, homogeneous surface film from AMPip-TFSI was beneficial to the cell life. During the first 15 cycles, the average Coulombic efficiency of the cell with AMPip-TFSI (97.31%) is higher than that with PMPip-TFSI (93.97%). By the result of improved Coulombic efficiency, it is confirmed again that the passivation of the film which successfully block continuous electrolyte decomposition during cycling. Furthermore, in order to scrutinize the origin and behavior of the cell impedance over many the cycles, AC impedances of the charged cell were measured after the 1st and the 10th cycles. The results are presented as Nyquist plots in Figure 5.

Two apparent distinct semicircles were observed in the all obtained spectra. The impedance results were fitted with the proposed equivalent circuit, which represent the lithium ion battery system, and are shown in the inset of Figure 5. It is comprised of $R_{electrolyte}$, which describes the resistance between the working and reference electrode, R_{film}, which is the resistance related to the transport of lithium through the electrochemically formed surface film on the cathode, and R_{ct}, which is the charge-transfer resistance of the lithium reaction. It is well known that the diameter of the high frequency range semicircle is related to lithium ion migration resistance through the passivation film (R_{SEI}), and the medium frequency semicircle corresponds to the charge-transfer resistance (R_{ct}) in combination with the capacitance terms of C_{film} (capacitance of surface film) and C_{dl} (double layer capacitance)[15,26–28]. The impedance results correlate well with the previous results; the increased resistance on $LiCoO_2$ introduced by the electrochemically formed surface films was not negligible when considering the total cell resistance. In detail, R_{SEI} of the cell with the PMPip-TFSI electrolyte increased with ongoing electrochemical charge/discharge cycles (fitted result: 1079 Ohm for the 1st cycle and 1253 Ohm for the 10th cycle, Figure 5a), which indicates that the derived film was unable to stabilize the surface of the electrode. In contrast, the value of R_{SEI} of the cell with AMPip-TFSI, once generated during the first cycle, was preserved during the following cycles as shown in Figure 5b (fitted result: 887 Ohm for the 1st cycle and 834 Ohm for the 10th cycle).

The thin and homogeneous surface film from AMPip-TFSI exhibited low and stable R_{SEI} during the impedance analysis and is in agreement with the high 1st discharge capacity of the cell with AMPip-TFSI (Figure 1). Considering the impedance behavior and

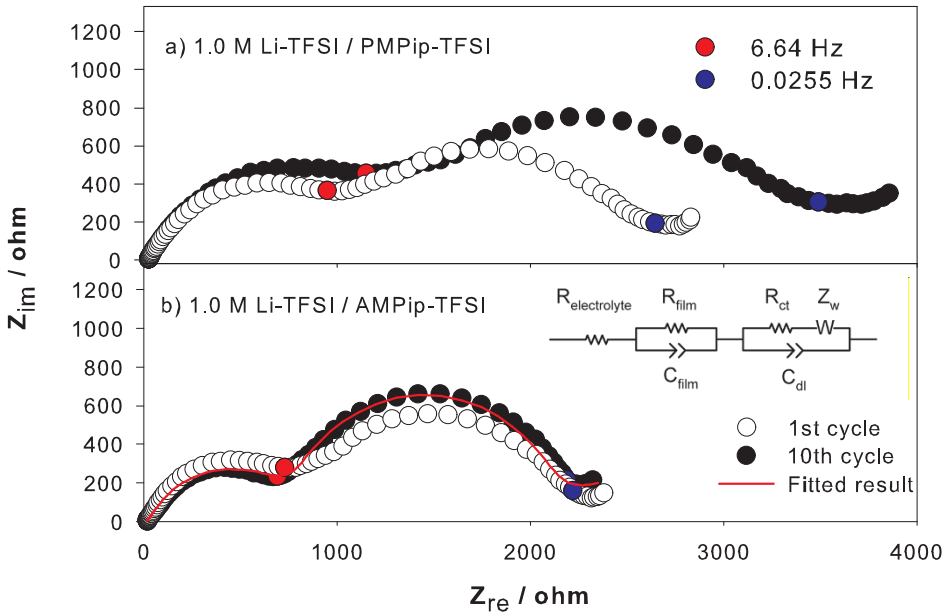

Figure 5 | AC impedance spectra of the $LiCoO_2$/Li cell taken from (a) 1.0 M PMPip-TFSI and (b) 1.0 M AMPip-TFSI. The measurements were conducted at the charged state (4.2 V vs. Li/Li$^+$) after the 1st and 10th charging.

obtained specific capacitances during cycling, it appears that the film derived from the electrochemical decomposition of AMPip-TFSI can sufficiently hinder the growth of resistance because of its high electrochemical stability. In the case of RTILs, we can minimally claim that the major reason for the deterioration of cell performance is due to an increase in cell resistance, which is influenced by the passivated film formed from electrolyte decomposition. From the same perspective, it can be concluded that the surface modification by electrochemical film passivation with AMPip-TFSI is highly effective in preventing surface reactions during the charge/discharge cycles. Although both electrolytes produce surface films, differences in their electrochemical effects arise from dissimilar film morphology.

Thermal properties. Figure 6 shows the DSC profiles of the fully charged cathode ($Li_{0.5}CoO_2$) containing the electrolytes. A large exothermic peak between 220 and 300°C is observed in all cases. The peak is associated with the vigorous interfacial reaction between the charged cathode material and electrolyte. Unstable delithiated cathode powder easily releases oxygen over the decomposition temperature range as described by the following route[29,30]:

$$Li_{0.5}CoO_2 \rightarrow {}^1/_2LiCoO_2 + {}^1/_6Co_3O_4 + {}^1/_6O_2 \quad (1)$$

Cobalt oxide can be further reduced to cobalt metal to release more oxygen through thermal decomposition. These thermal reactions are accelerated by the oxidation of the electrolyte because released oxygen can intensively and exothermically react with the electrolyte at the elevated temperature. The results of heating four different kinds of samples at a rate of $5^{\circ}C \cdot min^{-1}$ are summarized in Table 2. We used 1.0 M LiTFSI/ethylenecarbonate (EC) : diethylcarbonate (DEC) to represent a conventional carbonate-based electrolytes for LIBs and to examine the effects of Li-TFSI salt in the electrolyte. The cathodes with such carbonate electrolytes exhibit a large exothermic peak at 224.8°C and a heat capacity of 312.0 $J \cdot g^{-1}$ (Figure 6a and Table 2). In contrast, the charged cathode with the RTIL electrolytes clearly demonstrated improved thermal stability from the onset temperature, and their heat capacities were lower than those with the carbonate electrolytes. Specifically,

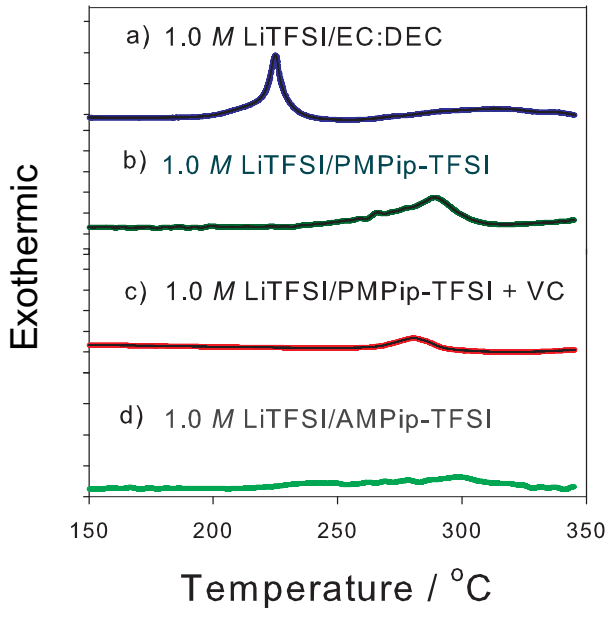

Figure 6 | DSC heating curves of fully charged $LiCoO_2$ with electrolytes: (a) 1.0 M LiTFSI/EC : DEC, (b) 1.0 M LiTFSI/PMPip-TFSI, (c) 1.0 M LiTFSI/PMPip-TFSI + VC, and (d) 1.0 M LiTFSI/AMPip-TFSI.

Table 2 | Temperature for the exothermic peaks and the heat capacity generated in the DSC curves shown in Fig. 6

Samples	Peak Temp (°C)	Enthalpy ($J\ g^{-1}$)
1.0 M LiTFSI/EC : DEC	224.8	312.0
1.0 M LiTFSI/PMPip-TFSI	289.2	234.3
1.0 M LiTFSI/PMPip-TFSI + 2 wt% VC	278.7	122.5
1.0 M LiTFSI/AMPip-TFSI	280.5	95.5

$Li_{0.5}CoO_2$ in 1.0 M LiTFSI/PMPip-TFSI produced a peak at 289.2°C with a heat capacity of 234.3 $J \cdot g^{-1}$ (Figure 6c and Table 2).

To elucidate the effects of the cathode-surface film on the thermal properties, we compared the charged cathode in RTIL-containing vinylenecarbonate (VC), which is a well-known additive for both cathodes and anodes. The primary exothermic peak of this combination appeared at a higher temperature, 278.7°C, and it had a lower heat capacity, 122.5 $J \cdot g^{-1}$, when compared to the values from the cell with PMPip-TFSI. The peak position was not significantly influenced, but the resulting heat capacity was remarkably decreased. The electrode containing the electrolyte with an allylic substituent produced the smallest exothermic peak at the highest temperature among all the tested samples. This indicates that the passivation film from AMPip-TFSI could effectively hinder the surface reaction between the electrode and electrolyte. We deduce that the high surface coverage of the allylic electrolyte plays a major role in preventing side reactions. The DSC thermograms measured for the RTIL groups presented higher thermal stabilities than those measured for the organic carbonate electrolytes. It is notable that the thermally stable RTILs affect the surface morphologies of the electrode, which can in turn influence surface reactivity when thermal decomposition occurs.

Discussion

The allyl moiety was incorporated into the piperidinium cation of RTIL (AMPip-TFSI) to electrochemically modify the surface of $LiCoO_2$ by using stable, electrochemical allylic radical formation. Surface modification as a result of the allyl group was confirmed by field-emission scanning electron microscopy (FE-SEM), transmission electron microscopy (TEM), and X-ray photoelectron microscopy (XPS), and the derived film from AMPip-TFSI was found to be more homogeneous and thinner (under 25 nm) than that from the PMPip-TFSI electrolyte. This novel surface film inhibited the decomposition of the electrolyte on the cathode, and the surface resistance for lithium diffusion between the electrolyte and electrode was preserved over several cycles. After surface modification by AMPip-TFSI, with comparing with the case of PMPip-TFSI, average Coulombic efficiency during the first 15 cycles was improved from 93.87 to 97.31%, which means the irreversible surface side reactions highly reduced. We not only observed an enhancement in the electrochemical stability, but also in the thermal stability. The onset temperature for the decomposition of active material was restrained by reducing the surface reactivity with electrolyte at elevated temperatures (PMPip-TFSI: 234.3 $J \cdot g^{-1}$ and AMPip-TFSI: 122.5 $J \cdot g^{-1}$). To summarize, allylic RTILs could result in the novel surface film that improves cyclability and increases thermal stability of LIBs.

Methods

RTIL Preparation. Two kinds of RTILs, with the same anion, TFSI, but different cations were prepared according to a previously reported methods[20]. The synthesized cations of RTILs were PMPip and AMPip. By repeated purification processes, the water and halide contents in the prepared electrolyte were controlled under 10 and 50 ppm, respectively. We added 1 M Li-TFSI (3 M, battery grade (>99.9%)) into prepared RTIL solvents to prepare the electrolytes for the LIB.

Electrochemical characterization. To prepare the slurry for the electrode, $LiCoO_2$ (JES-ECHEM), super-P (Timcal), and PVdF (Solvay) were mixed at a weight ratio of 89 : 6 : 5 in N-methylpyrrolidinone (Sigma-Aldrich, anhydrous, 99.5%). The slurry was coated onto the aluminum current collector, and the electrode plate was subsequently dried at 120°C under vacuum and pressed to reduce the contact resistance between particles. The electrodes were specially prepared for XPS analysis by embedding the $LiCoO_2$ powder onto a gold disk (Alfa Aesar, 0.25 mm, 99.95%) without a binder or conducting agent and pressed under 5000 psi for 30 min. Using those electrodes, 2032-type coin cells were fabricated by assembling a glassy filter (Advantec, GA-55, 0.21 mm thick, 0.6 μm pore) as the separator, the electrolytes, and a lithium foil as the counter electrode. The charge-discharge cycling test was conducted at 14 $mA \cdot g^{-1}$ (0.1 C) over the potential range of 3.0–4.2 V (vs. Li/Li^+) (model WBC-3000). Electrochemical impedance analysis was performed in a charged cell at a frequency range of 5 mHz–100 kHz with an AC amplitude of 10 mV.

Microscopic and spectroscopic analyses. For FE-SEM (JSM-6700F, JEOL), energy-filtered TEM (LIBRA 120, Carl Zeiss), and XPS (Sigma probe, Thermo) analyses, the cycled cells were dismantled in the glove box to avoid air contamination, and the electrodes were washed several times with dimethyl carbonate (DMC) to eliminate the residues from lithium salt and solvent. Hermetic vessels were used to transfer the prepared samples to the instrument chamber. The specimens were examined by TEM at an accelerating voltage of 120 kV. The XPS data were collected in an ultrahigh vacuum multipurpose surface analysis system operating under 10^{-10} mbar. The photoelectrons were excited by an AlKα (1486.6 eV) anode operating at a constant power of 100 W (15 kV and 10 mA), and the X-ray spot size was 400 μm.

Thermal analyses. For DSC measurements, electrodes were obtained from the coin-type cells and charged to 4.2 V (vs. Li/Li^+) at a current density of 14 $mA \cdot g^{-1}$ (0.1 C). The prepared electrodes were not subjected to any further treatment in order to preserve the conditions of the electrode in the cell during cycling. Approximately 5 mg of the electrode-containing electrolyte was hermetically sealed in a DSC pan. After assembling the pan for DSC, the temperature was ramped from 50 to 350°C at a rate of $10°C \cdot min^{-1}$ under Ar gas (DSC, DuPont Q2000).

1. Song, B. *et al.* High rate capability caused by surface cubic spinels in Li-rich layer-structured cathodes for Li-ion batteries. *Sci. Rep.* **3** (2013).
2. Yang, Y. *et al.* New Nanostructured Li_2S/Silicon Rechargeable Battery with High Specific Energy. *Nano Lett.* **10**, 1486–1491 (2010).
3. Recham, N. *et al.* A 3.6 V lithium-based fluorosulphate insertion positive electrode for lithium-ion batteries. *Nat. Mater.* **9**, 68–74 (2010).
4. Goodenough, J. B. & Kim, Y. Challenges for rechargeable Li batteries. *Chem. Mat.* **22**, 587–603 (2010).
5. Thackeray, M. M., Wolverton, C. & Isaacs, E. D. Electrical energy storage for transportation - Approaching the limits of, and going beyond, lithium-ion batteries. *Energ. Environ. Sci.* **5**, 7854–7863 (2012).
6. Mun, J. *et al.* The feasibility of a pyrrolidinium-based ionic liquid solvent for non-graphitic carbon electrodes. *Electrochem. Commun.* **13**, 1256–1259 (2011).
7. Yoon, W. S. *et al.* Structural study of the coating effect on the thermal stability of charged MgO-coated $LiNi_{0.8}Co_{0.2}O_2$ cathodes investigated by in situ XRD. *J. Power Sources* **217**, 128–134 (2012).
8. Amine, K. *et al.* Nanostructured Anode Material for High-Power Battery System in Electric Vehicles. *Adv. Mater.* **22**, 3052–3057 (2010).
9. Profatilova, I. A., Kim, S. S. & Choi, N. S. Enhanced thermal properties of the solid electrolyte interphase formed on graphite in an electrolyte with fluoroethylene carbonate. *Electrochim. Acta* **54**, 4445–4450 (2009).
10. Peled, E. The Electrochemical Behavior of Alkali and Alkaline Earth Metals in Nonaqueous Battery Systems–The Solid Electrolyte Interphase Model. *J. Electrochem. Soc.* **126**, 2047–2051 (1979).
11. Cho, J., Park, J., Lee, M., Song, H. & Lee, S. A polymer electrolyte-skinned active material strategy toward high-voltage lithium ion batteries: a polyimide-coated $LiNi_{0.5}Mn_{1.5}O_4$ spinel cathode material case. *Energ. Environ. Sci.* **5**, 7124–7131 (2012).
12. Lovelock, K. R. J. *et al.* Influence of Different Substituents on the Surface Composition of Ionic Liquids Studied Using ARXPS. *J. Phys. Chem. B* **113**, 2854–2864 (2009).
13. Yoon, H. *et al.* Lithium electrochemistry and cycling behaviour of ionic liquids using cyano based anions. *Energ. Environ. Sci.* **6**, 979–986 (2013).
14. Armand, M., Endres, F., MacFarlane, D. R., Ohno, H. & Scrosati, B. Ionic-liquid materials for the electrochemical challenges of the future. *Nat. mater.* **8**, 621–629 (2009).
15. Mun, J. *et al.* Surface Film Formation on $LiNi_{0.5}Mn_{1.5}O_4$ Electrode in an Ionic Liquid Solvent at Elevated Temperature. *J. Electrochem. Soc.* **158**, A453–A457 (2011).
16. Mun, J. *et al.* Comparative Study on Surface Films from Ionic Liquids Containing Saturated and Unsaturated Substituent for $LiCoO_2$. *J. Electrochem. Soc.* **157**, A136–A141 (2010).
17. Matsui, M., Dokko, K. & Kanamura, K. Dynamic behavior of surface film on $LiCoO_2$ thin film electrode. *J. Power Sources* **177**, 184–193 (2008).
18. Daheron, L. *et al.* Surface Properties of LiCoO2 Investigated by XPS Analyses and Theoretical Calculations. *J. Phys. Chem. C* **113**, 5843–5852 (2009).
19. Kim, M. G. & Cho, J. Reversible and high-capacity nanostructured electrode materials for li-ion batteries. *Adv. Funct. Mater.* **19**, 1497–1514 (2009).
20. Park, J. *et al.* Polyimide gel polymer electrolyte-nanoencapsulated $LiCoO_2$ cathode materials for high-voltage Li-ion batteries. *Electrochem. Commun.* **12**, 1099–1102 (2010).
21. Yim, T. *et al.* Synthesis and Properties of Pyrrolidinium and Piperidinium Bis (trifluoromethanesulfonyl) imide Ionic Liquids with Allyl Substituents. *Bull. Korean Chem. Soc* **28**, 1567 (2007).
22. Abe, K. *et al.* Additives-containing functional electrolytes for suppressing electrolyte decomposition in lithium-ion batteries. *Electrochimica Acta* **49**, 4613–4622 (2004).
23. Sakaebe, H. & Matsumoto, H. N-Methyl-N-propylpiperidinium bis(trifluoromethanesulfonyl)imide (PP13-TFSI) - novel electrolyte base for Li battery. *Electrochem. Commun.* **5**, 594–598 (2003).
24. Li, J. *et al.* Study of the storage performance of a Li-ion cell at elevated temperature. *Electrochim. Acta* **55**, 927–934 (2010).
25. Aurbach, D., Markovsky, B., Shechter, A., Ein-Eli, Y. & Cohen, H. A comparative study of synthetic graphite and Li electrodes in electrolyte solutions based on ethylene carbonate-Dimethyl carbonate mixtures. *J. Electrochem. Soc.* **143**, 3809–3820 (1996).
26. Gao, X. W. *et al.* $LiNi_{0.5}Mn_{1.5}O_4$ spinel cathode using room temperature ionic liquid as electrolyte. *Electrochimica Acta* **101**, 151–157 (2013).
27. Liu, J. & Manthiram, A. Understanding the Improvement in the Electrochemical Properties of Surface Modified 5 V $LiMn_{1.42}Ni_{0.42}Co_{0.16}O_4$ Spinel Cathodes in Lithium-ion Cells. *Chem. Mat.* **21**, 1695–1707 (2009).
28. Shaju, K. M. & Bruce, P. G. Nano-$LiNi_{0.5}Mn_{1.5}O_4$ spinel: a high power electrode for Li-ion batteries. *Dalton Trans.* **40**, 5471–5475 (2008).
29. MacNeil, D. D. & Dahn, J. R. The Reaction of Charged Cathodes with Nonaqueous Solvents and Electrolytes: I. $Li_{0.5}CoO_2$. *J. Electrochem. Soc.* **148**, A1205–A1210 (2001).
30. Larush, L. *et al.* On the thermal behavior of model Li-Li_xCoO_2 systems containing ionic liquids in standard electrolyte solutions. *J. Power Sources* **189**, 217–223 (2009).

Acknowledgments

The authors acknowledge the financial support from the National Research Foundation of Korea funded by the MEST (NRF-2010-C1AAA001-2010-0029065).

Author contributions

J.M., T.Y., S.L., J.R. and S.O. designed the study and experiment and co-wrote the paper. J.M., J.R. and S.O. have investigated the theme with respect of electrochemistry. T.Y. and Y.K. designed and synthesized the electrolyte. J.P. and S.L. worked on thermal analysis. J.M. and T.Y. conducted most of experiments and analyzed data and drafted the manuscript. S.O. critically reviewed, revised and finalized the manuscript. S.O. is guarantor of the paper.

Additional information

Supplementary information accompanies this paper at http://www.nature.com/scientificreports

Competing financial interests: The authors declare no competing financial interests.

How to cite this article: Mun, J. *et al.* Allylic ionic liquid electrolyte-assisted electrochemical surface passivation of $LiCoO_2$ for advanced, safe lithium-ion batteries. *Sci. Rep.* **4**, 5802; DOI:10.1038/srep05802 (2014).